

See discussions, stats, and author profiles for this publication at: <https://www.researchgate.net/publication/278790263>

Designing Composite Coatings That Provide a Dual Defense against Fouling

ARTICLE *in* LANGMUIR · JUNE 2015

Impact Factor: 4.46 · DOI: 10.1021/acs.langmuir.5b00888 · Source: PubMed

CITATION

1

READS

64

5 AUTHORS, INCLUDING:



Ya Liu

University of Pittsburgh

31 PUBLICATIONS 101 CITATIONS

[SEE PROFILE](#)



Xin Yong

Binghamton University

20 PUBLICATIONS 122 CITATIONS

[SEE PROFILE](#)



Olga Kuksenok

Clemson University

121 PUBLICATIONS 1,221 CITATIONS

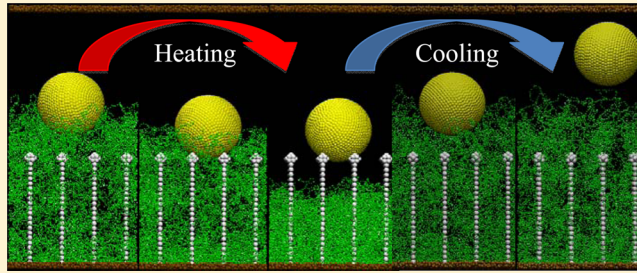
[SEE PROFILE](#)

Designing Composite Coatings That Provide a Dual Defense against Fouling

Ya Liu, Gerald T. McFarlin, IV, Xin Yong,[†] Olga Kuksenok, and Anna C. Balazs*

Chemical Engineering Department, University of Pittsburgh, Pittsburgh, Pennsylvania 15261, United States

ABSTRACT: Inspired by marine organisms that utilize spines and shape changes to prevent the biofouling of their surfaces, we use computational modeling to design a gel-based composite coating that provides a two-pronged defense mechanism against the fouling of the underlying substrate. Using dissipative particle dynamics (DPD) simulations, we construct a coating that encompasses rigid posts embedded in a thermoresponsive gel, which exhibits a lower critical solution temperature (LCST). When the gel is heated above its LCST, it collapses to expose the buried posts, which act as spines or spikes that prevent a solid particle from penetrating the layer. Moreover, we show that an imposed shear flow readily dislodges these particles and washes them away from the coated substrate. As the system dissipates heat and cools, the LCST gel expands, and this dynamic morphological change can also be harnessed to dislodge the adsorbed particles. Thus, both the exposed posts and the swelling gels can provide barriers to the penetration of particulates through the coating. In this manner, the coating provides a dual mechanism against the fouling of the substrate. This physical approach can be particularly beneficial because it does not require the release of any chemical substances that could have detrimental consequences to the environment.



I. INTRODUCTION

One of the challenges in creating antifouling coatings is devising means to prevent the adsorption of particulates onto surfaces without using chemicals that could ultimately be detrimental to the local environment.^{1–4} In order to establish more environmentally benign methods for preventing fouling, it is useful to consider the natural defense mechanisms utilized by marine organisms to clean their surfaces.^{5–7} The echinoderms (e.g., sea urchins) provide prime examples of marine organisms that are highly effective at preventing the settlement and growth of other organisms on their surfaces.^{6,7} The dermis of these marine organisms is typically covered with spines, which provide a physical barrier to the encroachment of biofoulers. Another distinctive feature of the echinoderms is that they can dynamically alter their shape and activate concealed defense mechanisms in response to the presence of a predator.⁸

Inspired by marine organisms who utilize responsive, multipronged defense mechanisms to prevent biofouling of their surfaces, we use computational modeling to design a gel-based composite film that provides a dual-defense mechanism against fouling. Figure 1 shows the components of our system: rigid posts that are embedded in a thermoresponsive gel, which is attached to a substrate. The gel depicted in green exhibits a lower critical solution temperature (LCST) (as displayed, for example, by poly(*N*-isopropylacrylamide)).^{9–12} Hence, when the gel is heated, it collapses and thereby exposes the buried posts, which act as spines or spikes that prevent the fouling agents from penetrating the layer. Thus, the exposed spikes provide one line of defense against the fouling of the substrate. Moreover, we show that, in the case where the particulates are perched on top of the exposed posts, an imposed shear flow

readily dislodges these particles and washes them away from the interface.

The second line of defense is provided by the gel itself. Namely, as the system dissipates heat and cools, the LCST gel begins to expand, and this dynamic morphological change can be harnessed to dislodge the particulates adsorbed on the layer. In other words, the gel's dynamic reconfiguration prevents particulates from reaching the substrate. In this context, it is worth recalling recent experimental studies where the stretching of a wrinkled film dislodged the fouling agents that were bound to the layer.⁷ Hence, a dynamic change in the structure of the film was sufficient to clean the surface. It is also worth recalling recent experiments where fouling agents were successfully dislodged from an elastomeric surface that was made to puff up and expand by pressurized air.¹³ The expansion of the thermoresponsive gel could behave in a conceptually analogous manner; here, temperature is used, rather than mechanical deformation, to drive dynamic structural changes in the film.

Thus, in this hybrid material, both the exposed posts and the swelling gels can provide barriers to the penetration of particulates through the coating. In this manner, the coating provides a dual mechanism against the fouling of the substrate. Below, we pinpoint the parameter space that yields the optimal antifouling behavior for this system. To do so, we use dissipative particle dynamics (DPD) simulations^{14–16} to model the components of the system and capture the dynamic

Received: March 9, 2015

Revised: May 17, 2015

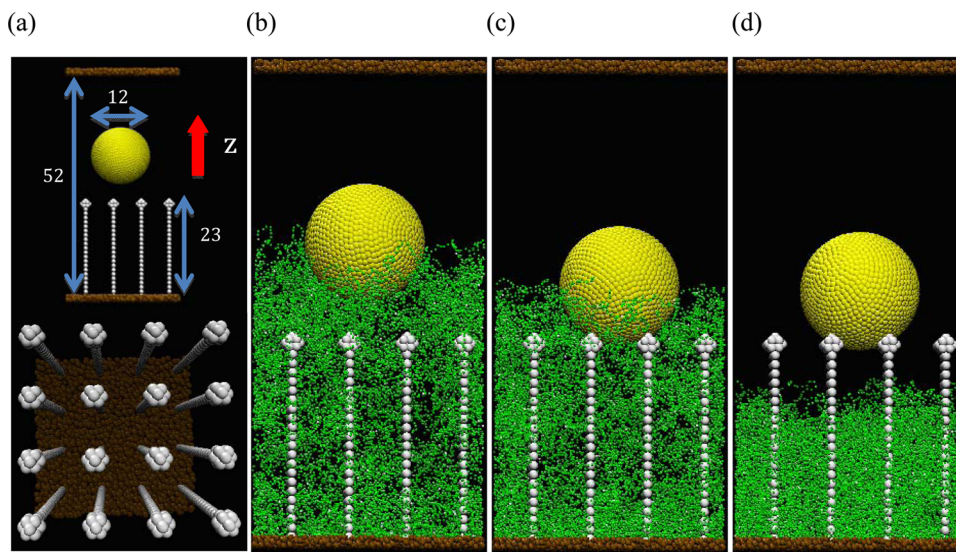


Figure 1. (a) Upper panel illustrates the geometric parameters set in the initial system. Lower panel is the top view of the posts arrangement. (b) Initial morphology of the system with the swollen gel, rigid posts, and particle at $T = 28\text{ }^\circ\text{C}$. (c) As the system temperature is increased to $T = 48\text{ }^\circ\text{C}$, the shrinking of the gel leads to the particle being caught by the posts at $t = 10^6$. (d) Late time morphology of the system at $t = 5 \times 10^6$. Here, $a_{pp} = 25$.

behavior of the hybrid material in the solution. DPD can be viewed as a coarse-grained molecular dynamics (MD) approach where clusters of molecules are represented by a single bead and the beads experience a soft-core repulsion (rather than the hard-core Lennard-Jones interaction commonly utilized in MD).^{14–16} Due to the latter attributes, DPD simulations can capture phenomena occurring on larger length and time scales than those which can be typically modeled with more atomistic MD simulations.^{17–19}

These studies are facilitated by our recently developed DPD model for thermoresponsive gels.²⁰ In particular, we developed a DPD approach that explicitly incorporates the temperature dependence of the polymer–solvent interactions in chemically cross-linked gels, allowing us to realistically model gels characterized by specific values of the polymer–solvent interaction parameter, $\chi_{ps}(T)$. We validated this model by accurately reproducing the volume phase transition of poly(*N*-isopropylacrylamide) (PNIPAAm) as a function of temperature.²⁰

Below, we detail our computational approach. We then describe how thermoresponsive LCST gels that conceal embedded posts can be utilized as effective antifouling coatings.

II. METHODOLOGY

II.A. Description of the Model. Our system is depicted in Figure 1a, which displays the array of rigid posts (in white) that are anchored to the substrate (brown beads). The posts are embedded in a thermoresponsive hydrogel (in green in Figure 1b) that exhibits lower critical solution temperature (LCST) behavior and, thus, swells at lower temperatures, T , and collapses at higher T . The fouling agent is modeled as a spherical particle (in yellow in Figure 1); in the initial configuration, there is no contact between the particle and posts. The entire system is immersed in a host solution.

To model the dynamic behavior of this system, we utilize DPD,^{14–16} which is a particle-based approach used to simulate the time evolution of a many-body system governed by Newton's equation of motion, $m \frac{dv_i}{dt} = f_i$. Each bead i in the system experiences a force f_i that is the sum of three pairwise

additive forces: $f_i(t) = \sum_j (F_{ij}^C + F_{ij}^D + F_{ij}^R)$, where the sum is over all beads j within a certain cutoff radius r_c from bead i . The three forces are the conservative force F_{ij}^C , drag or dissipative force F_{ij}^D , and random force F_{ij}^R . We describe each pairwise force below.

The conservative force is a soft, repulsive force given by $F_{ij}^C = a_{ij}(1 - r_{ij})\hat{r}_{ij}$, where a_{ij} measures the maximum repulsion between beads i and j , $r_{ij} = |\mathbf{r}_i - \mathbf{r}_j|/r_c$, and $\hat{r}_{ij} = (\mathbf{r}_i - \mathbf{r}_j)/|\mathbf{r}_i - \mathbf{r}_j|$. This soft-core force leads to a degree of overlap between neighboring beads and permits the use of larger time steps than those typically used in MD simulations. The repulsive parameters a_{ij} are given in terms of $k_B T$. We choose room temperature as the reference value; thus, $k_B T_0 = 1$ with $T_0 = 25\text{ }^\circ\text{C}$. The reduced temperature is introduced as $T^* = (T + 273.15)/(T_0 + 273.15)$; hence, $T^* = 1.077$ for $T = 48\text{ }^\circ\text{C}$ and $T^* = 1.01$ for $T = 28\text{ }^\circ\text{C}$. All repulsive parameters are listed in units of T^* (see Table 1).

The drag force is $F_{ij}^D = -\gamma \omega_D(r_{ij})(\hat{r}_{ij})(\hat{r}_{ij} \cdot \mathbf{v}_{ij})\hat{r}_{ij}$, where γ is a simulation parameter related to viscosity arising from the interactions between beads, ω_D is a weight function that goes to

Table 1. List of Interaction Parameters in Units of Reduced Temperature (T^*)

	solvent	particle	post	top wall	bottom wall	polymer gel
solvent	25	40	40	25	25	χ_{ps}
particle		25	a_{pp}	40	40	40
post				25	40	40
top wall					25	25
bottom wall						25
polymer gel						25

zero at r_{ij} and $\mathbf{v}_{ij} = \mathbf{v}_i - \mathbf{v}_j$. The random force is $\mathbf{F}_{ij}^R = \sigma\omega_R(r_{ij})\xi_{ij}\hat{\mathbf{r}}_{ij}$, where ξ_{ij} is a zero-mean Gaussian random variable of unit variance and $\sigma^2 = 2k_B T \gamma$. The value of γ is chosen to ensure relatively rapid equilibration of the system temperature and the numerical stability of the simulations for the specified time step.¹⁶ Finally, we use $\omega_D(r_{ij}) = \omega_R(r_{ij})^2 = (1 - r_{ij})^2$ for $r_{ij} < 1$.¹⁶

Each of these three pairwise forces conserves momentum locally; thus, DPD reproduces correct hydrodynamic behavior.^{14–16} The velocity-Verlet algorithm is applied to integrate the equations of motion in time. We take r_c as the characteristic length scale and $k_B T$ as the characteristic energy scale in our simulations. The corresponding characteristic time scale is then defined as $\tau = (mr_c^2/k_B T)^{1/2}$. The remaining simulation parameters are $\sigma = 3$ and $\Delta t = 0.02\tau$, with a total bead number density of $\rho_{sys} = 3$.¹⁶

We take the initial configuration of the gel to be a finite-sized tetrafunctional network with a diamond-like topology.²¹ The semiflexible polymer strands are modeled as a sequence of n DPD beads that are connected by harmonic bonds, with an interaction potential given by $E = 1/2(K_{bond}(r - r_0)^2) + K_{angle}(1 + \cos \theta)$.^{22,23} The first term in the latter expression characterizes the elastic energy with the elastic constant K_{bond} and the second term represents the bending energy with the rigidity parameter K_{angle} . Here, r_0 is the equilibrium bond length and θ is the equilibrium bond angle between two adjacent bonds. The bond and angle potentials of the gel are set, respectively, at $K_{bond} = 128$ and $K_{angle} = 4$ to prevent bond crossing and to produce a polymer concentration comparable to the experimental results for this gel.^{24,25} Consequently, the total force acting on each gel bead is equal to $\mathbf{f}_e + \mathbf{f}_b$, where $\mathbf{f}_e = -VE$ and \mathbf{f}_b is the DPD pairwise force.

Similar to the network modeled by Jha et al.,²¹ the finite-sized network contains cross-links, which are beads with a connectivity of four, and dangling ends, which are located on the surface of lattice and have a connectivity of less than four. In our study, the gel contains 15 488 beads and is periodic in the lateral (x and y) directions. This network consists of 540 strands, 247 cross-links, and 41 dangling ends.²⁰

To properly model the thermoresponsive behavior of this gel, we relate the repulsive parameter between a polymer and solvent bead, a_{ps} , to the Flory–Huggins parameter that characterizes the polymer–solvent interaction, χ_{ps} , as follows: $a_{ps} = a + k_B T \chi_{ps} / 0.306$.¹⁶ In studies of thermoresponsive gels (e.g., poly(*N*-isopropylacrylamide) PNIPAAm), it is typically assumed that χ_{ps} depends on temperature and polymer concentration.^{9–12} Hence, we assume that $\chi_{ps}(T, \varphi) = \chi_1(T) + \chi_2 \varphi_p$, where φ_p is the polymer volume fraction in the gel and $\chi_1(T) = (\delta h - T\delta s)/k_B T$, with δh and δs being the respective changes in enthalpy and entropy.^{9,26} Note that φ_p is calculated by $\varphi_p = \bar{\rho}_p / \bar{\rho}_{gel}$, where $\bar{\rho}_p$ is the time-averaged number density of the polymer beads and $\bar{\rho}_{gel}$ is the time-averaged total number density of the gel including the polymer and solvent beads. Here, we set $a = 25$ and choose $\delta h = -14.331 \times 10^{-14}$ erg, $\delta s = -5.452 \times 10^{-16}$ erg·K⁻¹, and $\chi_2 = 0.596$ to produce a continuous volume transition between $T = 30$ °C and 35 °C.^{16,27–31} In particular, with this choice of a_{ps} , we reproduce the experimentally observed temperature-induced volume phase transitions of the PNIPAAm gels.^{9,20,32}

The gel layer is attached via an adhesive interaction to the substrate (brown beads in Figure 1a). The effective attraction between the gel and substrate is modeled by setting interaction

parameter between the polymer beads in the gel and bottom wall, a_{gw} , at $a_{gw} = a_{ps} - 8$ so that the gel remains anchored to the wall in all our simulations.

The nondeformable spherical particle in Figure 1 is constructed from 3858 DPD beads that are uniformly dispersed on three spherical layers, with outer layer radius $R_p = 6$ and an interlayer spacing of 0.4. The total diameter of the particle is 12. The total force and torque acting on this particle is computed as the sum of the forces and torques on its constituent DPD beads. The corresponding number density of the particle shell is 12.2, which is sufficiently high to prevent penetration of the polymer beads into the sphere.

The posts are modeled as rigid polymers that encompass a fixed bond length of 0.5, and each post is 23 units in length. The 4 × 4 array of posts is anchored on the substrate with an interpost spacing of 6.15, as shown in Figure 1a. Each post is capped with a head that contains 10 DPD beads arranged in a regular structure based on the diamond cubic morphology (see lower image in Figure 1a). The lattice spacing in the head of the post is taken as 1, which ensures that the head density is close to the system density of $\rho_{sys} = 3$. These head groups prevent the penetration of the posts into the surface of the nondeformable particle even under high shear rates. In these studies, we vary the particle–post interaction a_{pp} from 25 to 45.

The top and bottom solid walls that bound the system in the z direction are modeled by solid beads (brown in Figure 1a), with a height $h = 1$ and a density $\rho_{wall} = 3$, having an amorphous structure. Bounce-back boundary conditions are applied at the fluid–solid interfaces to prevent the solvent and gel beads from penetrating into the walls and to produce no-slip boundary conditions with minimal interfacial density oscillations.³³ Periodic boundary conditions are applied along the x and y directions.

Shear is applied to the system by moving the upper wall of the simulation box at specified velocities. The shear rate $\dot{\gamma}$ takes the values 0, 0.0093, 0.019, and 0.028, which corresponds, respectively, to the velocity of the upper wall of 0, 0.5, 1, and 1.5.

Finally, the simulation box is 24.6 × 24.6 × 54 units in size and is filled with 70 224 solvent beads, maintaining the total density of the system at $\rho_{sys} = 3$. Four independent simulations are carried out for each parameter setup.

II.B. Comparison of Simulation Parameters to Physical Values. We can relate the dimensionless parameters to physical values through the value of the collective diffusion coefficient of the polymer network. If we assume that each solvent bead represents 10 water molecules,^{34,35} then a DPD solvent bead occupies a volume of 300 Å³ since a water molecule (of mass density 1 g/cm³) has a volume ~30 Å³. The total bead number density in our system is $\rho_{sys} = 3$, and using $\rho_{sys} = 3r_c^{-1}$ and the mass density of water, we obtain the unit length $r_c = 0.97$ nm and the characteristic mass $m = 180$ Da. By matching the mass density of a polymer bead in the simulation to the mass density of amorphous PNIPAAm (1.1 g/cm³), we find that a polymer bead represents 1.6 PNIPAAm monomers.²⁰

Knowing the characteristic length, mass, and energy, the time scale for the DPD simulation is calculated as $\tau_{intrinsic} = (mr_c^2/k_B T_0)^{1/2} = 8.3$ ps. It is known that conventional DPD produces accelerated dynamics due to the soft-core potential if the above intrinsic time scale is used.^{16,36,37} To obtain the correct characteristic time scale, we relate the collective diffusion coefficient of the polymer network in the simulations, $D_0^{sim} = 1.74 \times 10^{-2}$ nm²/τ_{DPD}, obtained from the swelling kinetics of

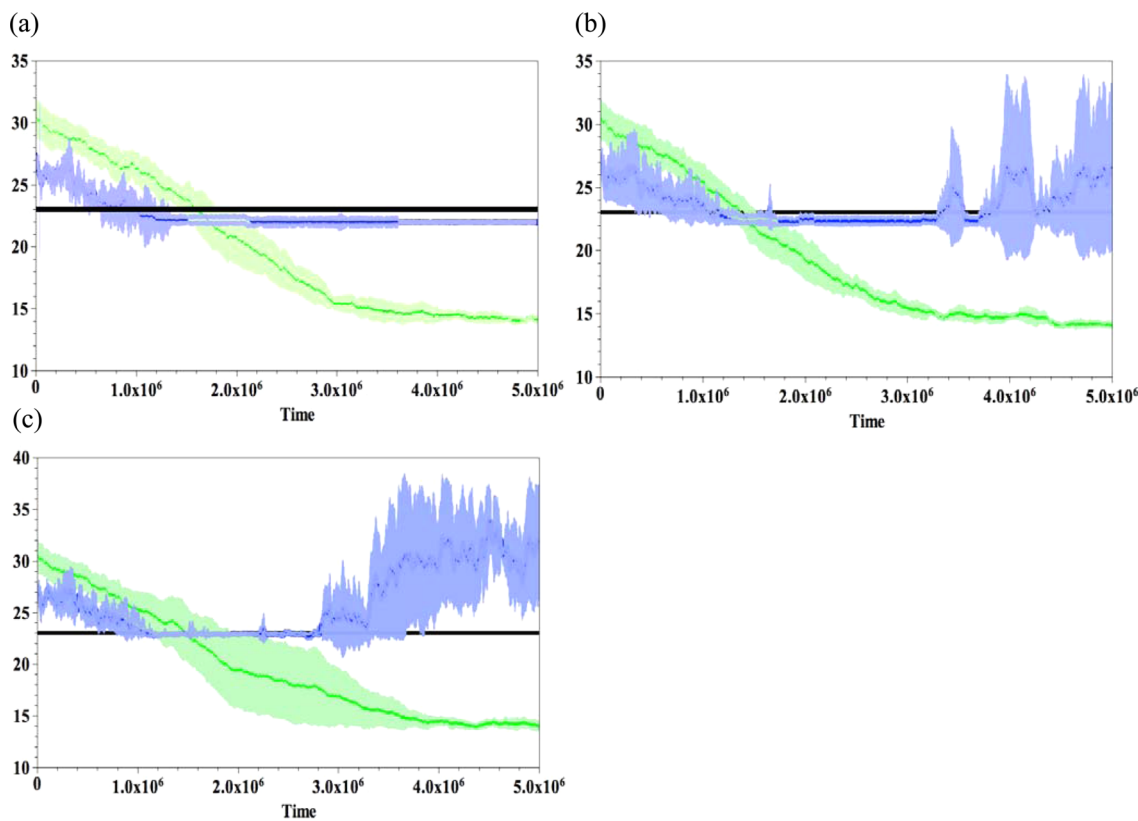


Figure 2. Temporal evolution of Z_c (blue), h_{gel} (green), and h_p (black) for different interactions between the particle and posts: (a) $a_{\text{pp}} = 25$, (b) $a_{\text{pp}} = 35$, and (c) $a_{\text{pp}} = 45$.

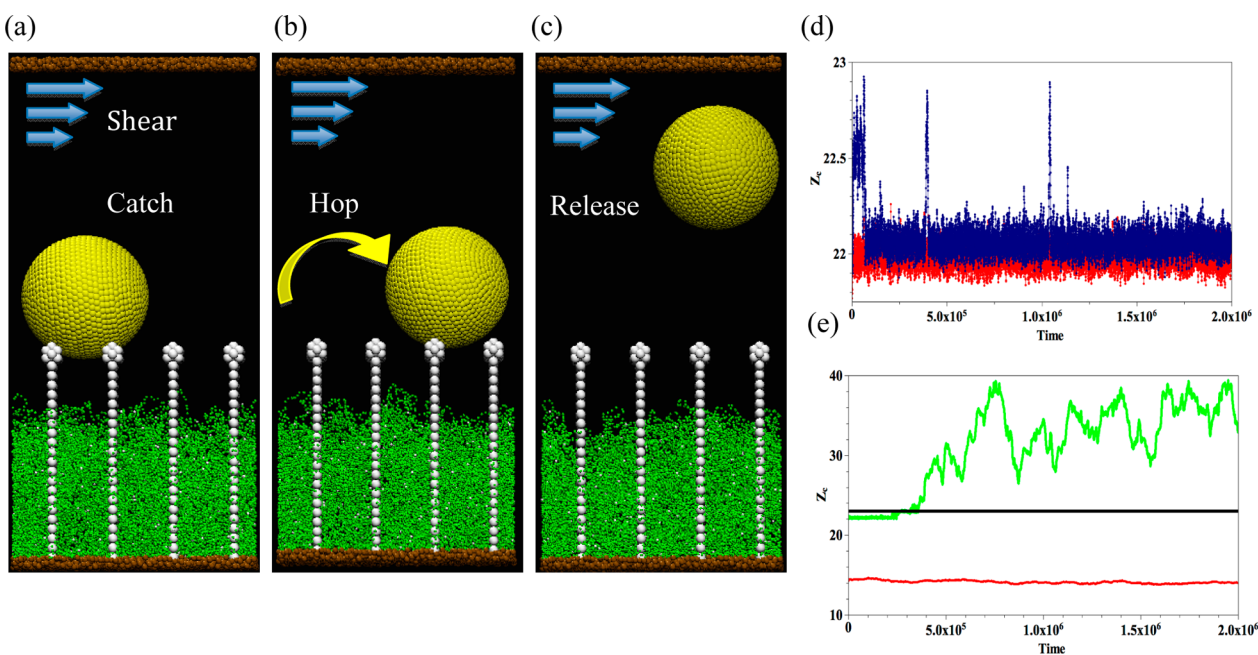


Figure 3. Illustration of the three states of the particle under the external shear: (a) catch, (b) hop, and (c) release. The initial morphology of the system is the same as that in (a). (d) Temporal evolution of Z_c for the state of catch (red) and hop (blue). (e) Temporal evolution of Z_c (green) for the state of release. Black and red curves correspond to the temporal evolution of h_p and h_{gel} , respectively.

the gel to experimental time scales $D_0^{\text{exp}} = 2 \times 10^{-11} \text{ m}^2/\text{s}$.³⁸ We thus obtain the following physical values for the simulation parameters: $\tau_{\text{DPD}} = 86 \text{ ns}$, the simulation box size is $23.9 \times 23.9 \times 52.38 \text{ nm}^3$, the post length is 22.3 nm, and the particle diameter is 10.44 nm. The maximum value of the applied shear

rate 0.028 corresponds to $\dot{\gamma} = 2.8 \times 10^7 \text{ s}^{-1}$.^{39,40} $K_{\text{bond}} = 128$ and $K_{\text{angle}} = 4$ correspond to 0.56 N/m and 4 $k_B T$, respectively.⁴¹

Finally, we note that the systems described herein have, to date, not been fabricated; hence, the findings presented below

can yield useful guidelines for creating coatings providing a dual mechanism against fouling. Notably, we have undertaken direct comparisons between our DPD simulation approach and corresponding experiments on polymer gels.⁴² In particular, we modeled gelation using atom transfer radical polymerization (ATRP) and successfully matched our simulation results to the experimental findings, thereby providing insight into the factors that affect the formation and binding of different gel layers within a multilayer structure.

III. RESULTS AND DISCUSSIONS

III.A. Defense Mechanism Provided by the Exposed Posts.

To illustrate the distinctive antifouling properties

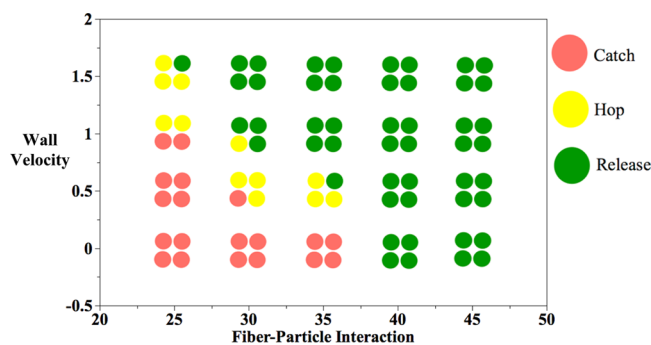


Figure 4. Phase diagram of the particle state as a function of the wall velocity and a_{pp} .

afforded by embedding rigid posts into thermoresponsive gels, we examine the behavior of a hydrophobic particle that is introduced above the LCST gel layer when the system is at a low temperature (i.e., below the phase transition temperature for the gel). Initially, the bottom bead on the spherical particle lies at a height $Z_c = 27$ from the substrate (Figure 1a). The gel is equilibrated at $T = 28$ °C (in the absence of a shear flow). The height of the gel layer, h_{gel} , is determined by averaging the z -component of the top gel beads; this procedure yields an equilibrium value of $h_{gel} \approx 30.4$ at $T = 28$ °C. Thus, the particle

is only in partial contact with the gel and does not touch the embedded posts, as can be seen in Figure 1b.

The entire system is relaxed for 10^3 time steps before the temperature is instantaneously increased to $T = 48$ °C. Since the gel exhibits LCST behavior, the layer collapses at the higher temperature and the equilibrium height of the polymer network is now equal to $h_{gel} \approx 14.2$. Note that, due to the temperature-dependence of the Flory–Huggins χ_{ps} parameter between the gel and solvent,⁹ at this temperature, the gel is effectively hydrophobic (i.e., $a_{ps} = 31$).

Notably, the hydrophobic particle remains localized at the gel–solvent interface. The reason for this behavior can be explained by the relative strength of repulsion between components dictated by the interaction parameters. As indicated in Table 1, the interaction parameter between the solvent beads ($a_{ss} = 25$) is lower than the polymer–solvent ($a_{ps} = 31$ for $T = 48$ °C) interaction parameter. Hence, the solvent–polymer contacts are less energetically favorable than the solvent–solvent contacts. The localization of particle on top of the gel layer reduces the number of unfavorable contacts in the system and thus minimizes the total free energy of the system. This energy minimization induces an effective attraction between the particle and the gel, driving the particle to remain localized on top of the gel layer (as seen in Figure 1b,c). (Additional simulations show that when the polymer–solvent interaction is held fixed at $a_{ps} = 25$ the particle no longer resides on the gel but, rather, is completely suspended in the solvent. With the solvent–solvent and gel–solvent interaction energies being identical, there is no enthalpic drive to minimize the gel–solvent contacts.)

When the height of the gel collapses below $h_{gel} < 23$, the rigid posts that were submerged within the gel coating now become exposed and thus come in contact with the particle. Since the spacing between the posts is less than the particle diameter, they act as spikes that prevent the particle from descending farther toward the bottom substrate. Because the particle and posts are both nondeformable, the sphere remains localized on the tips of posts, with just a few points of contact between these objects (see Figure 1d, where the postparticle interaction

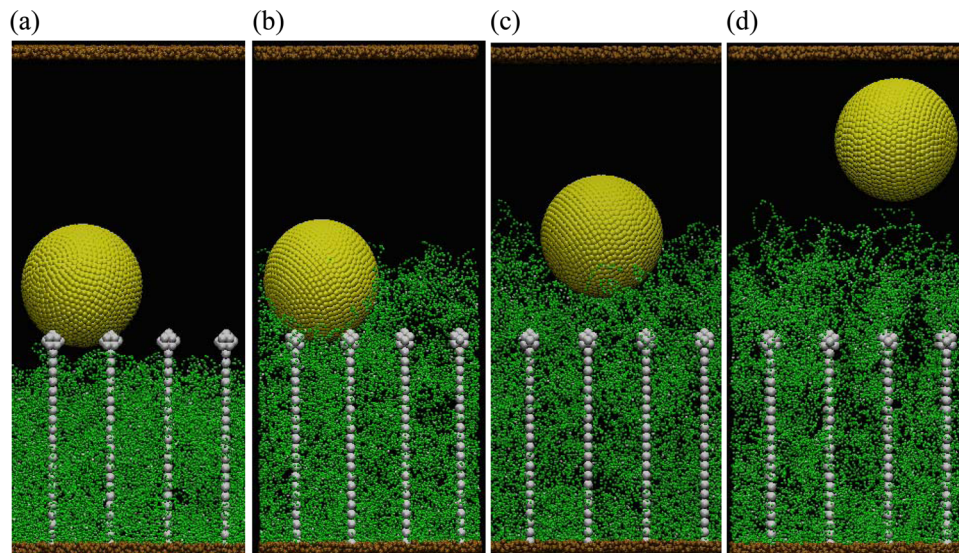


Figure 5. (a) Snapshot of the initial system. (b) Snapshot of the system at $t = 0.5 \times 10^6$ after the system was cooled to $T = 28$ °C. (c) Snapshot of the system at $t = 3.5 \times 10^6$ when the particle is released from the posts. (d) Snapshot of the system at $t = 5 \times 10^6$.

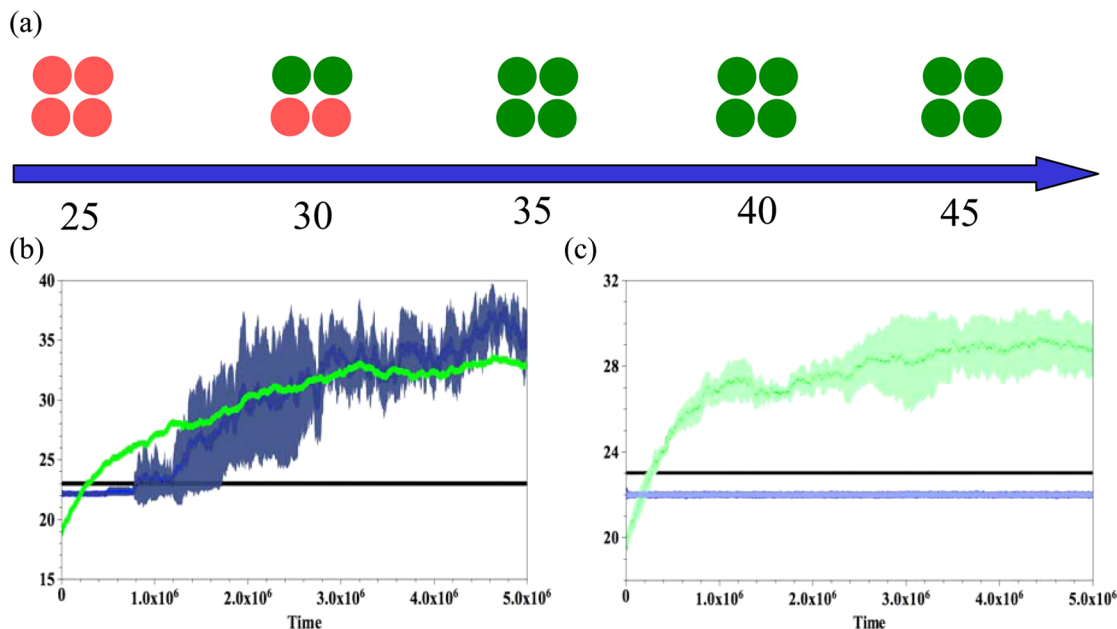


Figure 6. (a) Phase diagram of the particle state as a function of a_{pp} after the system was cooled to $T = 28$ °C. (b, c) Temporal evolution of Z_c (blue), h_{gel} (green), and h_p (black) for $a_{pp} = 35$ and $a_{pp} = 25$, respectively.

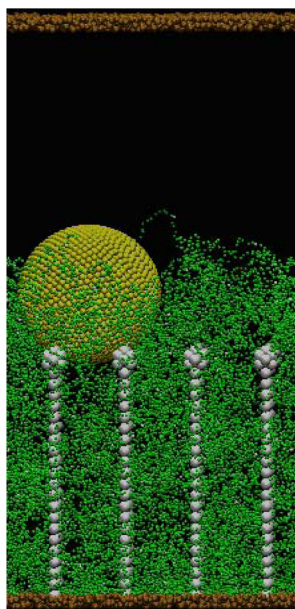


Figure 7. Snapshot of the system for $a_{pp} = 25$ at $t = 5 \times 10^6$ after the system was cooled to $T = 28$ °C.

parameter is fixed at $a_{pp} = 25$). As we show below, the particle could be readily dislodged by an imposed shear flow.

Before introducing an external flow (see further below), we investigate how the enthalpic interactions between the particle and posts could be altered to destabilize the particle's position on the posts. To this end, we set the particle–post repulsion parameter to the following values: $a_{pp} = 25$, 35, and 45. Since the particle–solvent interaction is $a_{pas} = 40$ (see Table 1), the effective particle–post interaction is strongly attractive at $a_{pp} = 25$, weakly attractive at $a_{pp} = 35$, and repulsive at $a_{pp} = 45$. Figure 2a–c shows the temporal evolution of the gel height h_{gel} (in green) and the particle position Z_c (in blue) for these respective cases as the temperature is instantaneously increased to $T = 48$ °C (on the structure equilibrated at $T = 28$ °C).

The height of the post's tip, $h_p = 23$, does not vary with time and is plotted in black as a reference point. The data is obtained by averaging over four independent simulations; the vertical bars about each data point represent the corresponding error bars. The gel height is determined by the temperature-dependent gel–solvent interactions; at $T = 48$ °C, h_{gel} reaches the equilibrium value of $h_{gel} \approx 14.2$ in approximately 4×10^6 time steps (see Figure 2). As noted above, when the gel is swollen above the posts, the particle remains localized at the gel–solvent interface. Hence, the particle position Z_c decreases in a similar manner for all three values of a_{pp} until the posts are exposed and the particle contacts with the post tips at $t \approx 1.1 \times 10^6$. (Due to the spacing between the posts, the position of bottom bead on the particle, $Z_c \approx 22$, lies lower than h_p .) When $t > 1.1 \times 10^6$, the gel keeps collapsing and detaches from the particle. Thereafter, the dynamics of the particle depends on a_{pp} .

At a weak repulsion parameter, $a_{pp} = 25$ (Figure 2a), the particle position clearly plateaus at $Z_c \approx 22$, indicating that this sphere remains localized on the posts, bound by the relatively attractive tips. For the case of weaker attraction, $a_{pp} = 35$, (Figure 2b), the particle is attached to the post when $t > 3.2 \times 10^6$. The value of Z_c , however, displays large fluctuations when $t > 3.2 \times 10^6$ and h_{gel} approaches the equilibrium value for $T = 48$ °C. The latter behavior is consistent with our observations that the particle becomes detached from the posts in two of the four simulations. At this temperature, thermal fluctuations in the system promote the particle's Brownian motion, which can dominate over the weak attractive interaction and thus lead to particle detachment. When the particle–post interaction is strongly repulsive at $a_{pp} = 45$ (Figure 2c), then $Z_c > h_p$ for $t > 2.8 \times 10^6$, suggesting that the particle is repelled from the posts and is diffusing freely in the solvent.

III.B. Removing the Particle by an Imposed Shear. Imposed flows have commonly been used to remove fouling agents from substrates. Here, we determine the ability of an imposed shear to dislodge the particle from the posts when the temperature is fixed at $T = 48$ °C. Figure 3a shows the initial

configuration of the system when the particle is attached to the posts by the weak repulsion (which corresponds to effectively strong attraction, $a_{pp} = 25$) and the gel is equilibrated at $T = 48^\circ\text{C}$. After the system is relaxed for 10^3 time steps, we introduce the shear flow (see Methodology); in these studies, we vary both the magnitude of the applied shear and the value of a_{pp} . (For each set of parameters, we run four independent simulations, which start from different initial configurations.) Since the gel height (represented by the red line in Figure 3e) lies below the posts' tips and the temperature is kept constant, the enthalpic interactions between the particle and the gel do not affect the motion of the particle.

We observed that the particle can exhibit three types of behavior: catch, hop, or release. If the attached particle remains localized on a given set of posts in the presence of the flow, then we refer to this state as catch; Figure 3a exemplifies the structure of this state. If, however, the particle is no longer bound to one specific set of posts but rather moves from one set to another, so that it remains restricted to the post tips, then the state is referred to as hop (Figure 3b). Finally, if the particle is detached from the posts and released into the solution with no point of contact with the posts, then it is in the release state (Figure 3c).

We distinguish among the three states by monitoring the particle position Z_c as shown in Figure 3d,e. In the catch state, $Z_c \approx 22$ and the particle exhibits very small fluctuations about this value (red in Figure 3d). For the hop state, the value of Z_c (blue in Figure 3d) is close to the height of the post's tip $h_p = 23$; the relatively large spikes correspond to the state where the particle hops among the different tips. Note that the fluctuations of Z_c for the catch states (red curve) and the blue curve during the time that a particle is between hops and effectively bound to a post are of similar magnitude (≈ 0.15). Figure 3e illustrates the state of release, where Z_c (the green curve) become larger than h_p .

By varying the magnitude of the shear rate and a_{pp} , we generate the phase map in Figure 4, which reveals the optimal combination of parameters to achieve the different states and, in particular, indicates favorable conditions for expelling the particle from the surface. Each dot in a grouping corresponds to one of the four independent simulations. Red, yellow, and green refer to the catch, hop, and release states, respectively. As a point of reference, we first consider the behavior of the system in the absence of an applied shear: all of the particles are in the catch state (red dot) when the particle–post interactions are relatively attractive ($a_{pp} < 40$), and all of the particles are in the release state for the neutral ($a_{pp} = a_{pas}$) and repulsive interactions ($a_{pp} > 40$). (Recall that the particle–solvent interaction is characterized by $a_{pas} = 40$.) The release of the particle with the neutral interaction is due to thermal fluctuations at the higher temperature ($T = 48^\circ\text{C}$).

As the velocity of the upper wall is increased to 0.5 (corresponding to an increase in the shear rate), we observe the hop state in three of the four simulations for the case of the relatively weak attraction ($a_{pp} = 30$), indicating that the shear starts to dislodge the particles from the posts. For even weaker attraction ($a_{pp} = 35$), the particle is no longer bound to specific posts and we observe the release state in one simulation and the hop state in the remaining three simulations.

As the wall velocity is increased to 1, the particle is released for $a_{pp} \geq 35$ and no catch state is observed for $a_{pp} = 30$. For the strong attraction with $a_{pp} = 25$, the shear promotes the particle

mobility and two hop states are detected; for the other two simulations, the particles remain in the catch state.

When the strongest shear (=1.5) is applied, all of the particles are in the release state for $a_{pp} \geq 30$. For the strong attraction ($a_{pp} = 25$), the release state is observed in just one of the cases; the particle is in the hop state for the other three cases.

These findings indicate the distinctive features of this dual-defense system that are enabled by exposing the posts. Namely, the posts not only sterically inhibit the particles from reaching the substrate but also, due to the low number of particle–post contacts, enable the fouling agent to be readily removed from the surface by an imposed flow. Below, we describe the antifouling behavior that can be achieved by exploiting the dynamic behavior of the gel in this composite.

III.C. Defense Mechanism Provided by the Expanding Gel. The system was designed so that the polymer gel can also play an active role in removing the fouling particle. In particular, as the system cools, the expansion of the LCST gel can provide sufficient repulsion to dislodge the particle from the layer, as illustrated in Figure 5. The image in Figure 5a shows the initial morphology of the system, with the particle attached to the post by a strong particle–post attraction ($a_{pp} = 25$). The system is quenched to the temperature $T = 28^\circ\text{C}$ without shear; thus, the polymer gel experiences reversible swelling, as shown in Figure 5b. As the gel expands, the number of points of contact between the gel and the particle are significantly increased, thus enhancing the repulsive excluded volume interactions between the polymer layer and the particle. (Note that for this simulation the initial configuration for the simulation was taken from a temperature where the gel is close to but does not actually make contact with the particle.) If this repulsion is stronger than the adhesion between the particle and the posts, then the particle can be detached from the posts (Figure 5c) and driven into the bulk solution (Figure 5d).

As in the previous section, we distinguish the particle behavior by its final state and generate the corresponding phase map as the function of a_{pp} in Figure 6a. As can be seen from this map, the swelling gel can successfully remove the particle for $a_{pp} \geq 35$; this behavior can also be seen from the simulation results in Figure 6b. As the gel height increases, the particle position Z_c (blue) increases, becoming comparable to h_{gel} (green). For relatively strong particle–post adhesion ($a_{pp} = 30$), two cases of release are observed.

It is noteworthy, however, that release state is not found for $a_{pp} = 25$ because the excluded volume repulsion is not sufficiently strong to overcome the strongest particle–post attraction considered here. As shown in Figure 6c, Z_c (blue) remains constant even when the gel interface (green) grows above the particle, i.e., $h_{gel} > h_p$; this behavior suggests that particle is in the catch state, and the observation is consistent with the snapshot of the system at $t = 5 \times 10^6$ (Figure 7).

IV. CONCLUSIONS

Using computational modeling, we isolated the parameter range in which the gel–post composite provides the optimal dual-defense mechanism against the fouling of the surface. This system has the potential to be effective not only when the temperature is increased so that the gel collapses to expose the spikes but also as the system cools and the gel swells to effectively expel the particles from the layer. The proposed dual-defense system offers the distinct advantage that it embodies two complementary means of expelling particulates

from the surface and hence can provide a more robust method of preventing fouling than an approach that relies on a single mechanism.

We anticipate that fouling particulates adhered to the gel layer will detach from the surface upon localized heating, as their attachment strength will significantly decrease due to the following factors. In particular, (1) as the gel shrinks below the posts, the particles land on the post tips, resulting in a drastically reduced areal contact with the surface, (2) the posts can be made nonadhesive to reduce the interaction with the particles, (3) the process can be cycled to push these particles away by the expanding gel, as shown in Figure 5, and (4) the poorly attached particles can be removed from the surface by applying shear.

Finally, we note that the proposed approach relies on physical mechanisms rather than the release of chemical agents to inhibit the fouling. This is particularly appealing since chemical approaches could have unexpected and unwanted environmental consequences; thus, methods that exploit dynamic physical behavior could ultimately provide more efficacious means of preventing fouling.^{1–4}

AUTHOR INFORMATION

Corresponding Author

*E-mail: balazs@pitt.edu.

Present Address

[†](X.Y.) Department of Mechanical Engineering, Binghamton University, State University of New York, Binghamton, New York 13902-6000, United States.

Notes

The authors declare no competing financial interest.

ACKNOWLEDGMENTS

A.C.B. gratefully acknowledges financial support from ONR grant no. N00014-11-1-0641.

REFERENCES

- (1) Banerjee, I.; Pangule, R. C.; Kane, R. S. Antifouling coatings: recent developments in the design of surfaces that prevent fouling by proteins, bacteria, and marine organisms. *Adv. Mater.* **2011**, *23*, 690–718.
- (2) Guardiola, F. A.; Cuesta, A.; Meseguer, J.; Esteban, M. A. Risks of using antifouling biocides in aquaculture. *Int. J. Mol. Sci.* **2012**, *13*, 1541–60.
- (3) Thomas, K. V.; Brooks, S. The environmental fate and effects of antifouling paint biocides. *Biofouling* **2010**, *26*, 73–88.
- (4) Meyer, B. Approaches to prevention, removal and killing of biofilms. *Int. Biodeterior. Biodegrad.* **2003**, *51*, 249–253.
- (5) Campbell, A. C.; Rainbow, P. S. The role of pedicellariae in preventing barnacle settlement on the sea-urchin test. *Mar. Behav. Physiol.* **1977**, *4*, 253–260.
- (6) Ralston, E.; Swain, G. Bioinspiration—the solution for biofouling control? *Bioinspiration Biomimetics* **2009**, *4*, 015007.
- (7) Epstein, A. K.; Hong, D.; Kim, P.; Aizenberg, J. Biofilm attachment reduction on bioinspired, dynamic, micro-wrinkling surfaces. *New J. Phys.* **2013**, *15*, 095018.
- (8) McKenzie, J. D.; Grigolava, I. V. The echinoderm surface and its role in preventing microfouling. *Biofouling* **1996**, *10*, 261–72.
- (9) Hirotsu, S. Softening of bulk modulus and negative Poisson's ratio near the volume phase transition of polymer gels. *J. Chem. Phys.* **1991**, *94*, 3949.
- (10) Quesada-Pérez, M.; Maroto-Centeno, J. A.; Forcada, J.; Hidalgo-Alvarez, R. Gel swelling theories: the classical formalism and recent approaches. *Soft Matter* **2011**, *7*, 10536–10547.
- (11) Hirotsu, S. Phase transition of a polymer gel in pure and mixed solvent media. *J. Phys. Soc. Jpn.* **1987**, *56*, 233–242.
- (12) Erman, B.; Flory, P. J. Critical phenomena and transitions in swollen polymer networks and in linear macromolecules. *Macromolecules* **1986**, *19*, 2342–2353.
- (13) Shivapooja, P.; Wang, Q.; Orihuela, B.; Rittschof, D.; Lopez, G. P.; Zhao, X. Bioinspired surfaces with dynamic topography for active control of biofouling. *Adv. Mater.* **2013**, *25*, 1430–1434.
- (14) Hoogerbrugge, P. J.; Koelman, J. M. V. A. Simulating microscopic hydrodynamic phenomena with dissipative particle dynamics. *Europhys. Lett.* **1992**, *19*, 155–160.
- (15) Español, P.; Warren, P. Statistical mechanics of dissipative particle dynamics. *Europhys. Lett.* **1995**, *30*, 191–196.
- (16) Groot, R. D.; Warren, P. B. Dissipative particle dynamics: bridging the gap between atomistic and mesoscopic simulation. *J. Chem. Phys.* **1997**, *107*, 4423.
- (17) Long, D.; Sotta, P. Stress relaxation of large amplitudes and long timescales in soft thermoplastic and filled elastomers. *Rheol. Acta* **2007**, *46*, 1029–1044.
- (18) Moeinzadeh, S.; Barati, D.; He, X.; Jabbari, E. Gelation characteristics and osteogenic differentiation of stromal cells in inert hydrolytically degradable micellar polyethylene glycol hydrogels. *Biomacromolecules* **2012**, *13*, 2073–86.
- (19) Raos, G.; Casalegno, M. Nonequilibrium simulations of filled polymer networks: searching for the origins of reinforcement and nonlinearity. *J. Chem. Phys.* **2011**, *134*, 054902.
- (20) Yong, X.; Kuksenok, O.; Matyjaszewski, K.; Balazs, A. C. Harnessing interfacially-active nanorods to regenerate severed polymer gels. *Nano Lett.* **2013**, *13*, 6269–74.
- (21) Jha, P. K.; Zwanikken, J. W.; Detcheverry, F. A.; de Pablo, J. J.; Olvera de la Cruz, M. Study of volume phase transitions in polymeric nanogels by theoretically informed coarse-grained simulations. *Soft Matter* **2011**, *7*, 5965–5975.
- (22) Masoud, H.; Alexeev, A. Controlled release of nanoparticles and macromolecules from responsive microgel capsules. *ACS Nano* **2012**, *6*, 212–219.
- (23) Pan, W.; Fedosov, D.; Karniadakis, G.; Caswell, B. Hydrodynamic interactions for single dissipative-particle-dynamics particles and their clusters and filaments. *Phys. Rev. E* **2008**, *78*, 046706.
- (24) Nikunen, P.; Vattulainen, I.; Karttunen, M. Reptational dynamics in dissipative particle dynamics simulations of polymer melts. *Phys. Rev. E* **2007**, *75*, 036713.
- (25) Karatrantos, A.; Clarke, N.; Composto, R. J.; Winey, K. I. Topological entanglement length in polymer melts and nanocomposites by a DPD polymer model. *Soft Matter* **2013**, *9*, 3877–3884.
- (26) Flory, P. J. *Principles of Polymer Chemistry*; Cornell University Press: Ithaca, NY, 1953.
- (27) Chang, H.-Y.; Lin, Y.-L.; Sheng, Y.-J.; Tsao, H.-K. Multilayered polymersome formed by amphiphilic asymmetric macromolecular brushes. *Macromolecules* **2012**, *45*, 4778–4789.
- (28) Groot, R. D.; Madden, T. J. Dynamic simulation of diblock copolymer microphase separation. *J. Chem. Phys.* **1998**, *108*, 8713.
- (29) Hellweg, T.; Dewhurst, C. D.; Brückner, E.; Kratz, K.; Eimer, W. Colloidal crystals made of poly(N-isopropylacrylamide) microgel particles. *Colloid Polym. Sci.* **2000**, *278*, 972–978.
- (30) Guo, J.; Liang, H.; Wang, Z. G. Coil-to-globule transition by dissipative particle dynamics simulation. *J. Chem. Phys.* **2011**, *134*, 244904.
- (31) Soto-Figueroa, C.; Rodríguez-Hidalgo, M. d. R.; Vicente, L. Dissipative particle dynamics simulation of the micellization–demicellization process and micellar shuttle of a diblock copolymer in a biphasic system (water/ionic-liquid). *Soft Matter* **2012**, *8*, 1871.
- (32) Schild, H. G. Poly(N-isopropylacrylamide): experiment, theory and application. *Prog. Polym. Sci.* **1992**, *17*, 163–249.
- (33) Fedosov, D. A.; Pivkin, I. V.; Karniadakis, G. E. Velocity limit in DPD simulations of wall-bounded flows. *J. Comput. Phys.* **2008**, *227*, 2540–2559.

- (34) Fuchslin, R. M.; Fellermann, H.; Eriksson, A.; Ziolk, H. J. Coarse graining and scaling in dissipative particle dynamics. *J. Chem. Phys.* **2009**, *130*, 214102.
- (35) Spaeth, J. R.; Kevrekidis, I. G.; Panagiotopoulos, A. Z. A comparison of implicit- and explicit-solvent simulations of self-assembly in block copolymer and solute systems. *J. Chem. Phys.* **2011**, *134*, 164902.
- (36) Symeonidis, V.; Karniadakis, G. E.; Caswell, B. Schmidt number effects in dissipative particle dynamics simulation of polymers. *J. Chem. Phys.* **2006**, *125*, 184902.
- (37) Junghans, C.; Praprotnik, M.; Kremer, K. Transport properties controlled by a thermostat: an extended dissipative particle dynamics thermostat. *Soft Matter* **2008**, *4*, 156–161.
- (38) Nikoobakht, B.; El-Sayed, M. A. Preparation and growth mechanism of gold nanorods (NRs) using seed-mediated growth method. *Chem. Mater.* **2003**, *15*, 1957–1962.
- (39) Segà, M.; Sbragaglia, M.; Biferale, L.; Succi, S. Regularization of the slip length divergence in water nanoflows by inhomogeneities at the angstrom scale. *Soft Matter* **2013**, *9*, 8526.
- (40) Moseler, M. Formation, stability, and breakup of nanojets. *Science* **2000**, *289*, 1165–1169.
- (41) K_{bond} can be estimated as $k_{\text{B}}T/r_c^2$. Using room temperature $T = 25^\circ\text{C}$, $k_{\text{B}}T = 4.11 \times 10^{-21} \text{ J}$, and $r_c = 0.97 \text{ nm}$, we find that $K_{\text{bond}} = 128$ corresponds to 0.56 N/m . K_{angle} has the dimensions of energy and, thus, $K_{\text{angle}} = 4$ is equivalent to $4k_{\text{B}}T$.
- (42) Yong, X.; Simakova, A.; Averick, S.; Gutierrez, J.; Kuksenok, O.; Balazs, A. C.; Matyjaszewski, K. Stackable, covalently fused gels: repair and composite formation. *Macromolecules* **2015**, *48*, 1169–1178.